Renal vascular inflammation induced by Western diet in ApoE-null mice quantified by 19F NMR of VCAM-1 targeted nanobeacons

ARTICLE *in* NANOMEDICINE: NANOTECHNOLOGY, BIOLOGY, AND MEDICINE · FEBRUARY 2009

Impact Factor: 6.16 · DOI: 10.1016/j.nano.2008.12.002 · Source: PubMed

Available online at www.sciencedirect.com
ScienceDirect
Nanomedicine: Nanotechnology, Biology, and Medicine xx (2009) xxx–xxx
nanomedicine
www.nanomedjournal.com

Renal vascular inflammation induced by Western diet in ApoE-null mice quantified by ^{19}F NMR of VCAM-1 targeted nanobeacons

Richard Southworth, PhD,[a,1] Megan Kaneda, BSc, MS,[b,1] Junjie Chen, PhD,[b] Lei Zhang, BSc, MS,[b] Huiying Zhang, MD,[b] Xiaoxia Yang, PhD,[b] Reza Razavi, MD,[a] Gregory Lanza, MD, PhD,[b] Samuel A. Wickline, MD[b,*]

[a]*Division of Imaging Sciences, King's College London, The Rayne Institute, St. Thomas' Hospital, London, UK*
[b]*Cardiovascular Division, Washington University School of Medicine, St. Louis, Missouri, USA*

Abstract We have designed multifunctional nanoparticulate reporter bioprobes capable of targeting vascular cell adhesion molecule 1 (VCAM-1), which is up-regulated in numerous inflammatory processes. These perfluorocarbon-cored nanoparticles emit a unique ^{19}F magnetic resonance (MR) signature, providing the potential to localize and quantify VCAM-1 expression in early atherosclerosis. Nanoparticle-VCAM-1 targeting specificity was confirmed by *in vitro* binding and competition studies. ApoE-null and control C57-BL6 mice (n = 6/group), fed a Western diet for 35 weeks, were injected i.v. with targeted or non-targeted nanoparticles. After two hours, kidneys were excised and prepared for analysis. ApoE-null kidneys exhibited increased VCAM-1-targeted nanoparticle content over healthy controls by ^{19}F MR spectroscopy (36.5+8.8 vs. 9.3+2.2 × 10^8/g, $P < .05$), which correlated with increased VCAM-1 staining (2.5 ± 1.3% vs. 0.9 ± 0.3%, $P < .05$); their relative biodistributions were confirmed by fluorescence microscopy and MR imaging. These molecular imaging agents offer new approaches for detection, quantification, and longitudinal evaluation of early inflammation utilising ^{19}F MR spectroscopy and imaging.

Key words: Molecular imaging; Nanoparticles; Inflammation; VCAM; Magnetic resonance

Introduction

Inflammation accompanying hyperlipidemia is a recognized causative factor in the development and progression of atherosclerosis in patients with acute and chronic vascular syndromes.[1,2] However, the etiological role of these factors in incipient renal disease that may be associated with atherosclerosis is not clear. In experimental models of atherosclerosis, focal renal mesangial expansion in association with expression of adhesion molecules (e.g., the vascular cell adhesion molecule, VCAM-1) and macrophage infiltration has been reported.[3] In patients with type II diabetes, a strong inverse relationship exists between plasma VCAM-1 content and glomerular filtration rate.[4] Furthermore, plasma VCAM-1 is increased in patients with chronic renal failure.[5] However, the overall involvement of the kidney and the potential impact of such inflammatory mediators on renal structure and function in response to hyperlipidemia in the early stages of the disease process are not well characterized.

The ability to address these questions both experimentally and clinically could be facilitated by the development of a

Received 28 May 2008; accepted 15 December 2008.
This work was supported by grants from the National Institutes of Health (HL073646, CA119342) and NHLBI grant 5 R01HL078631-04.
Wickline and Lanza; equity in and consulting relationships with Kereos, Inc.
[1] These authors contributed equally to the work.
*Corresponding author. Cardiovascular Division, Washington University School of Medicine, St. Louis, Missouri, USA.
E-mail address: saw@howdy.wustl.edu (S.A. Wickline).

1549-9634/$ – see front matter © 2009 Elsevier Inc. All rights reserved.
doi:10.1016/j.nano.2008.12.002

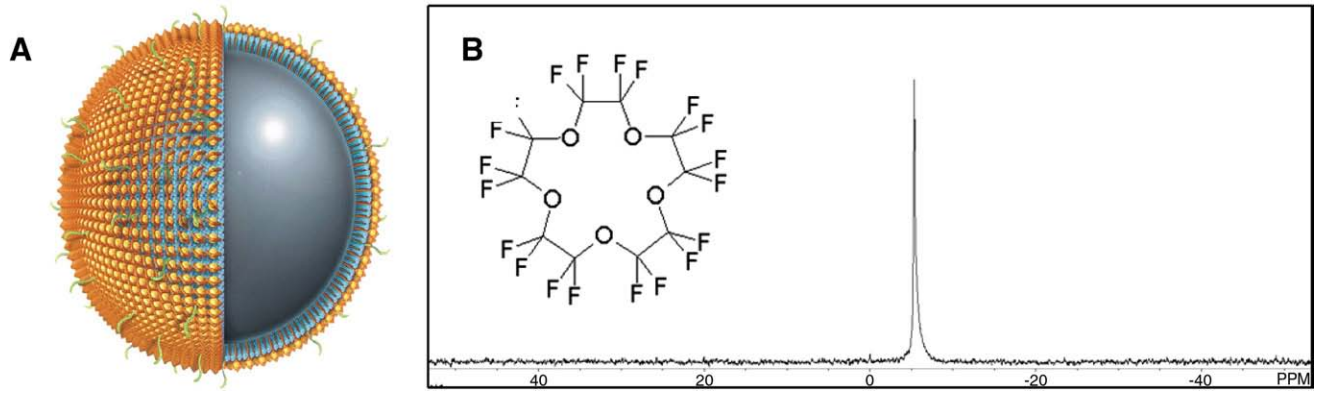

Figure 1. **(A)** Schematic of the nanobeacon structure. The structure is a lipid-encapsulated, liquid perfluorocarbon nanoparticle, nominal diameter 250nm, functionalised with homing ligands in the outer phospholipid monolayer (shown in green), and provide MR contrast by either a potential 90,000 Gd^{3+} nucleus/nanoparticle payload on its surface (shown in gold), or a 100M ^{19}F/nanoparticle payload in its core. Each crown ether molecule in the core contains 20 equivalent fluorine nuclei **(B)**, all contributing to a single NMR peak.

biomarker that was both specific to renal inflammation and readily quantifiable across the entire organ to gauge the extent and severity of the disease process. To that end, here we describe an approach that employs targeted nanobeacons that can be localized specifically to molecular markers of inflammation in the kidney, providing a unique, quantifiable, and non-invasive readout of the prevalence of relevant biomarkers using magnetic resonance spectroscopy (MRS) and/or imaging (MRI). To do so, we attached a targeting ligand specific for VCAM-1 to a perfluorocarbon-based nanoparticle that carries sufficient ^{19}F fluorine in its core to yield a MRS signal proportionate to the expression of the vascular inflammatory marker (Figure 1). We used this biomarker construct to quantify endothelial VCAM-1 expression in the intact kidneys of cholesterol-fed $ApoE^{-/-}$ mice to show that early endothelial activation is widespread, and particularly evident in the glomerulus, and occurs prior to any significant derangement in renal function or structure. These data suggest a role for this unique, specific, and quantifiable nanobeacon as a harbinger of evolving renal damage under diverse conditions, and as an agent for targeted drug delivery and disease management.

Methods

Preparation and analysis of targeted nanoparticles

Liquid PFC nanoparticles were formulated using methods previously developed in our laboratories.[6] Briefly, the emulsions comprised 20% (v/v) perfluoro-15-crown-5-ether (CE), 1.5% (w/v) of a surfactant/lipid co-mixture, and 1.7% (w/v) glycerine in distilled, deionised water. To permit fluorescence detection of particle binding, all emulsions contained 0.135 mol% rhodamine (1,2-dioleoyl-sn-glycero-3-phosphoethanolamine-N-(lissamine rhodamine B sulphonyl) (Avanti Polar Lipids, Inc., Alabaster, AL, USA) in the surfactant layer. To attach a targeting ligand to the nanoparticles, 0.09mol% N-[{w-[4-(p-maleimidophenyl) butanoyl]amino} poly(ethylene glycol)2000] 1,2-distearoyl-sn-glycero-3-phosphoethanolamine (MPB-PEG-DSPE) was added to the surfactant comixture. A VCAM-1 targeting peptide (VHPKQHRGGSGC) previously reported by Kelly et al[7] suspended in 6 mmol/L EDTA was and added to the lipid film to react at a 1:1 molar ratio of peptide to MPB-PEG-DSPE under nitrogen at 37°C. The reaction between the maleimide group on the MPB-PEG-DSPE and the thiol group on the peptide resulted in a thioether linkage. The mixture of surfactant components, PFC, and water was then sonicated and emulsified at 20,000 PSI for 4 min in an ice bath (S110 Microfluidics emulsifier, Microfluidics, Newton, MA). Particle size analysis by laser light scattering (Malvern Instruments, UK) measured sizes of 353.4 nm (polydispersity = 0.392). To calculate conjugation efficiency, emulsion samples were centrifuged at 3000g for 5 minutes to pellet the nanoparticles, and the peptide concentration in the supernatant measured by standard BCA protein assay. Our conjugation efficiency was 87.9% +/− 0.075. We calculate that approximately 870 peptides are bound to each nanoparticle.

In vitro analysis of targeted nanoparticles

To assess the specificity of our VCAM-1-targeted nanoparticles, we performed binding and competition experiments using murine endothelial 2F-2B cells, which express large numbers of VCAM-1 on their surface.[8] 2F-2B cells were maintained in DMEM supplemented with 10% fetal bovine serum (Gibco) and 1mmol/L sodium pyruvate in a humidified 5% CO_2 incubator. For confocal imaging, 25,000 cells were seeded on 0.17mm thick Delta TPG culture dishes (Bioptechs Inc, Butler, PA) and incubated with 1μL of either targeted or non-targeted nanoparticles in 1mL optimemI (Gibco) for 2 hours. Competition experiments were conducted by adding 0.5 mg/ml anti-VCAM-1 antibody to 1μL of targeted nanoparticles in 1mL optimemI and incubated as before. Cells were fixed with a 4% paraformaldehyde solution and washed with PBS. Images were

acquired with a Zeiss confocal microscope using a rhodamine filter set.

Animal experimental protocol

ApoE$^{-/-}$ and C57BL6 mice (n = 6/group) received a high cholesterol diet (Harlan Teklad, Madison Wis; 0.2% Cholesterol) for 35 weeks. At the end of the diet, mice were injected with targeted or non-targeted nanoparticles (1μL/g) via the tail vein. After allowing 2 hours for nanoparticle circulation and targeting, the animals were terminally anaesthetised (ketamine and xylazine 87 and 12mg/kg respectively), heparinised, and exsanguinated by 3 sequential infusions of 20mL heparinised saline via the left ventricle. Both kidneys and a liver sample (approximately 0.2g) were excised for subsequent analysis. One kidney was mounted in OCT medium and rapidly frozen in liquid nitrogen for histology and immunostaining; the other kidney and the liver sample were stored in saline-filled vials on ice for MR spectroscopy and imaging. The experimental and humane animal care protocols were approved by the animal care committee of the Washington University School of Medicine.

Immunohistological analysis

Expression of VCAM-1, the endothelial specific marker Platelet/endothelial cell adhesion molecule 1 (PECAM-1), and the macrophage antigen Mac-2 were determined using monoclonal antibodies to VCAM-1 (clone 429, BD Biosciences, San Jose, CA), PECAM-1 (clone TLD-3A12, BD Biosciences, San Jose, CA) and Mac-2 (clone M3/38 eBioscience, San Diego, CA) at dilutions of 1/200, 1/1500, and 1/2000 respectively. The antibodies were developed using the ImmPRESS Ig peroxidase kit and VIP Substrate Kit (Vector Laboratories, Burlingame, CA) with methyl green nuclear staining.

Quantitative analysis of VCAM-1, PECAM-1, and macrophage expression (Mac-2) were performed on six ApoE$^{-/-}$ and six C57/BL6 mice kidneys. For each kidney section, three different 1.3 x 1.0mm^2 cortical regions were imaged on a Nikon 800E microscope and digitized with a CCD camera. Tissue areas exhibiting positive staining (purple colour) were automatically detected using a custom-designed colour-based segmentation program written in Matlab (The Mathworks Inc. MA). For analysis, the thresholds for edge detection and colour intensity segmentation were held equivalent for all sets of slides to allow rational comparison among targeted, non-targeted, and control tissues. The ratio of positive-stained to non-stained area on each section was calculated for comparison among groups.

MR Spectroscopic quantification and imaging of nanoparticle binding

MR spectroscopy and imaging was performed on an 11.7T Varian *UNITY*-INOVA scanner using a custom-designed 5mm 4-turn solenoid RF coil. For ^{19}F signal calibration and quantification, an internal reference of 10μL 1% perfluorooctylbromide (PFOB) in a capillary tube was included in each vial. This PFOB signal is distinct from that of the crown ether (CE) in the nanoparticles (Figure 2), providing a readily identifiable spectral peak representing a known quantity of ^{19}F for calibration of CE signal intensity versus concentration.[9] ^{19}F MR spectroscopy (number of averages = 64, 90^o flip angle, acquisition time: 2 min) was performed for quantification of total nanoparticle accumulation in each tissue sample using a spin-echo sequence. To minimize variations in [O_2] that can potentially affect signals from perfluorocarbons,[10] samples were maintained in equilibrium with ambient air during data collection, and a TR time of 2 sec was used to ensure the recovery of ^{19}F magnetisation in each repetition (i.e., T_1~800ms for the CE in nanoparticles, so that T_2>3xT_1). A standard curve of relative peak areas corresponding to a range of CE and PFOB emulsion concentrations was generated, from which absolute nanoparticle numbers were calculated per tissue wet weight. *MR Imaging*: Kidneys from ApoE$^{-/-}$ and C57/BL6 mice which had been injected with VCAM-1-targeted nanoparticles, were inserted into vials filled with saline, placed in custom-built double-frequency tuneable solenoid RF coils, and imaged using standard spin-echo sequences. *Imaging parameters:* Multi-slice ^{1}H images: TR, 1 s; TE, 40 ms; slice thickness, 1mm; field of view, 4 × 2 cm^2; data matrix, 128 × 128; in-plane resolution, 312 × 156μm^2; number of averages, 1. ^{19}F images: TR, 0.5 s; TE, 18 ms; slice thickness, 20 mm; field of view, 4 × 2 cm^2; data matrix, 64 × 64 interpolated 128 × 128; in-plane resolution, 624 ×

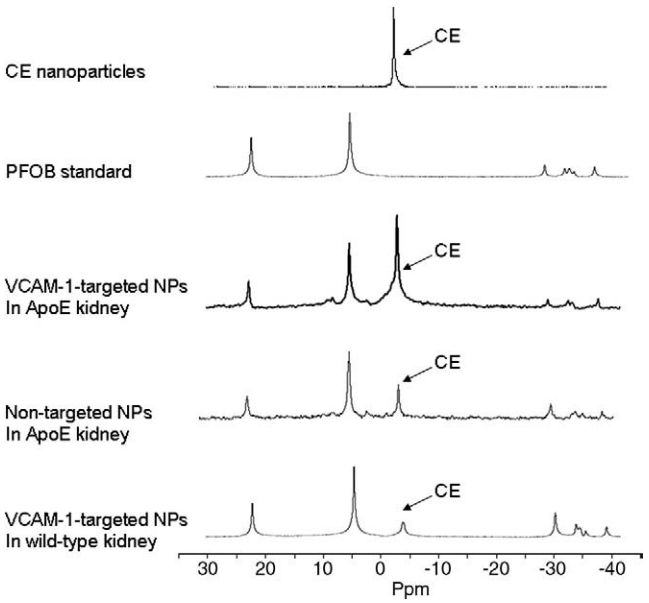

Figure 2. Representative ^{19}F NMR spectra of crown-ether containing nanoparticles (CE, 1%, 10μl) the perfluorooctylbromide internal standard (PFOB, 1%, 10μl), and whole kidneys (with internal PFOB standard) from ApoE$^{-/-}$ and wild-type mice injected with VCAM-1 targeted or non-targeted nanoparticles (1μl/g) as indicated. Spectra represent 64 averages, 90° flip angle. ppm: parts per million.

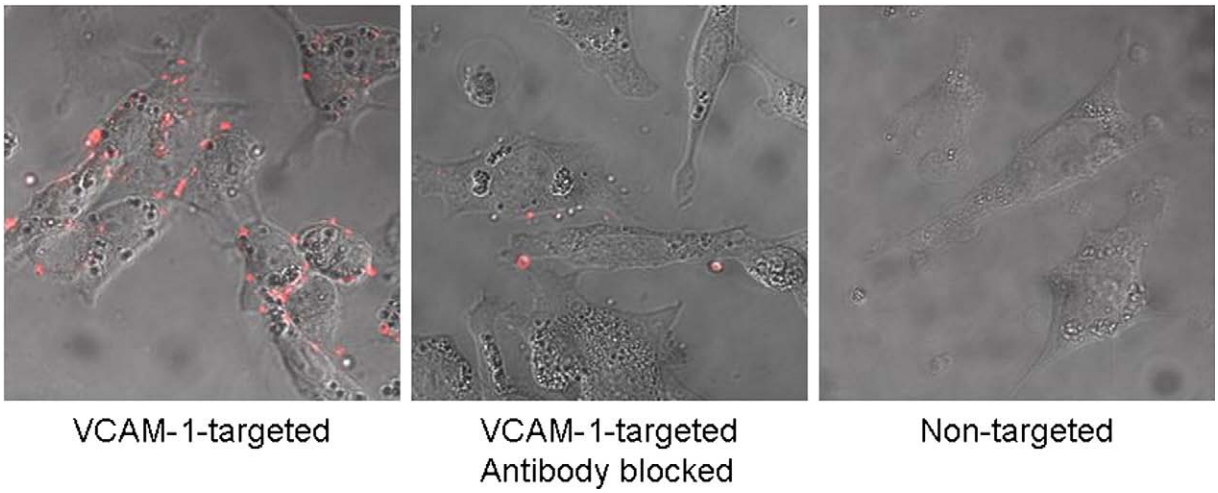

Figure 3. Specificity of the nanobeacons to cell surface VCAM-1. Nanoparticle location was visualised by fluorescence microscopy by rhodamine signal. VCAM-1-targeted nanobeacons bind to murine endothelial 2F-2B cells (left), while non-targeted nanobeacons do not (right); targeted nanobeacon binding is inhibited by competition with anti-VCAM-1 mAbs (middle).

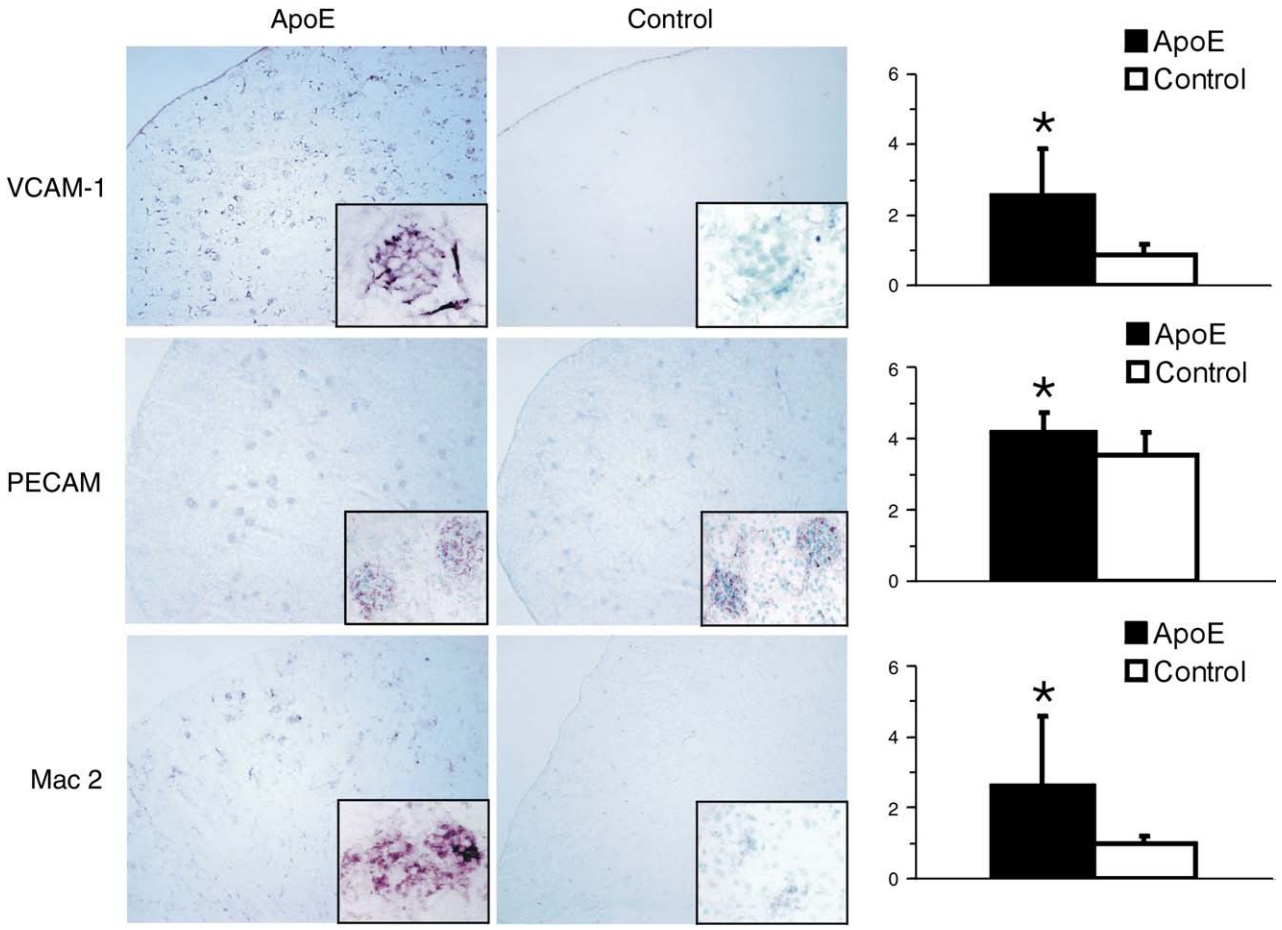

Figure 4. The ApoE$^{-/-}$ kidney is characterised by significant up-regulation of VCAM-1 expression and a marked infiltration of macrophages into the glomeruli. Quantitative analysis of VCAM-1, PECAM-1 (as an endothelial cell marker), and Mac-2 (a macrophage-specific marker) expression were performed in ApoE-null and control kidneys. For each kidney section, three cortical regions imaged on a Nikon 800E microscope and digitized with a CCD camera. Positive staining (purple colour) was quantified using a custom-designed color-based segmentation program written in Matlab (The Mathworks Inc. MA). Data represent mean (n = 6 ± SD). *represents $P < .05$.

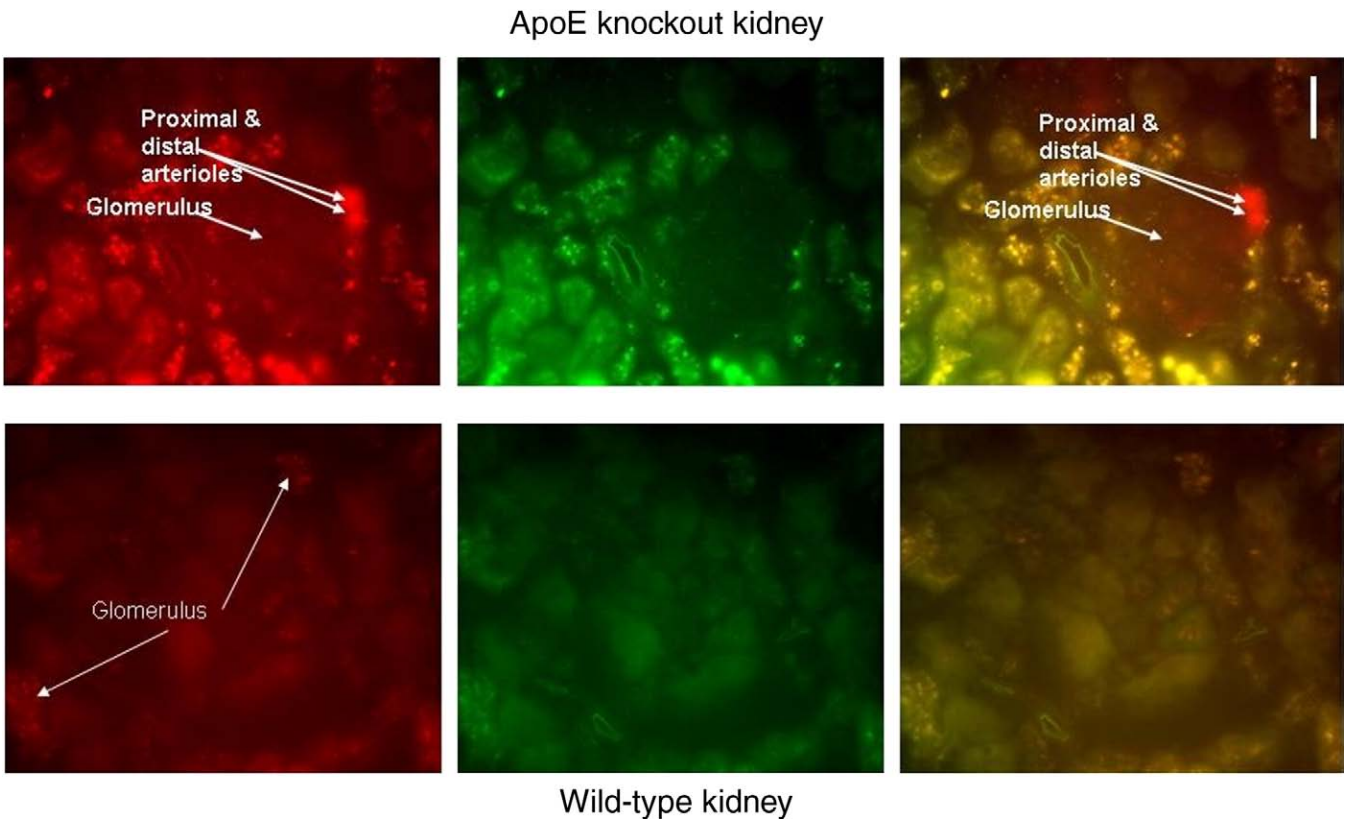

Figure 5. Nanobeacon targeting to VCAM-1, visualised by fluorescence microscopy. Representative micrographs are from an ApoE$^{-/-}$ mouse kidney (top) and a wild-type control kidney (bottom), fixed 2 hours after injection of VCAM-1-targeted, rhodamine-labelled nanoparticles. Colour panels represent (from left to right) red fluorescence (rhodamine + autofluorescence), green fluorescence (autofluorescence only), and composite images to distinguish rhodamine fluorescence (red) from autofluorescence (yellow). Scale bar = 100mm.

312μm^2; number of averages, 1024. All ^{19}F images were subjected to identical Wiener filtering to achieve noise reduction. Voxels with a signal intensity of greater than twice the standard deviation were defined as positive for ^{19}F to produce a nanoparticle distribution map throughout each kidney.

Since the liver is the principal clearance organ for these nanoparticles, we used ^{19}F NMR spectroscopy to quantify liver nanoparticle content to confirm successful injection, as detailed above. Animals with a liver nanoparticle content of less than 50% of the mean value for the entire study group were deemed to have not been successfully injected, and were excluded from analysis (approximately 5% of animals used). They were replaced with further animals which had been successfully injected to maintain an n of 6/group.

Statistical analysis

Data are expressed as mean ± SE. Comparison of ^{19}F MR data among ApoE$^{-/-}$ and control animals treated with targeted and non-targeted nanoparticles was performed using two-way analysis of variance with Bonferroni post-test intergroup comparisons. Comparison of histology-defined VCAM-1, Mac-2, or PECAM expression between ApoE$^{-/-}$ and control kidneys was performed using un-paired two-tailed student t-test. A P-value of <.05 was considered statistically significant.

Results

Specificity of nanobeacon VCAM-1 targeting in vitro

The binding of nanoparticles to the surface of mouse endothelial 2F-2B cells was clearly visible by fluorescence microscopy (Figure 3). Such binding was blocked by co-incubation with anti-VCAM-1 antibody, and did not occur when the targeting ligand was not present, confirming that nanoparticle binding is ligand-mediated, and VCAM-1-specific.

Immunohistological characterisation of the ApoE$^{-/-}$ kidney

VCAM-1 staining was evident in the glomeruli and arterioles of ApoE$^{-/-}$ kidney, and was significantly greater than that observed in control kidney when expressed as a percentage of total tissue area (2.5 ± 1.4% vs 0.9 ± 0.3%, $P <$ .05, Figure 3). This increased VCAM-1 expression was evident in glomerular endothelial cells and Bowman's capsule, and in arterioles and venules. In control kidneys,

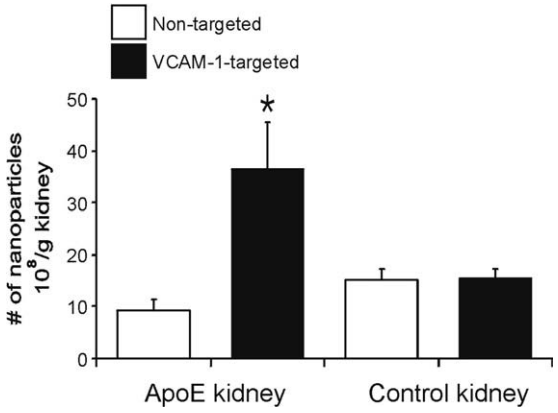

Figure 6. Absolute quantification of nanoparticle targeting to VCAM-1 in ApoE$^{-/-}$ and control kidneys, calculated from ^{19}F NMR spectra. Data represent mean (n = 6 ± SEM). *represents significantly different from all other groups ($P < .05$, 2-way ANOVA with Bonferroni post-test).

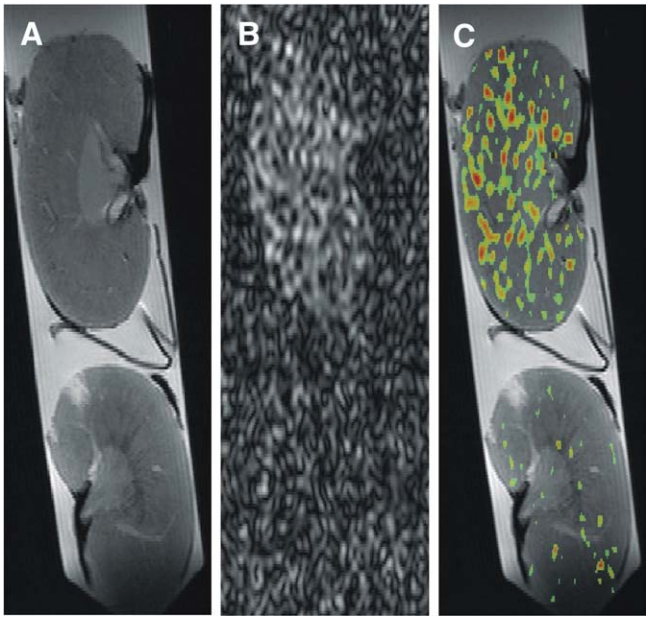

Figure 7. A representative ^{1}H MR image showing **(A)** structural detail, **(B)** ^{19}F MR image, and **(C)** a composite ^{1}H/^{19}F image showing VCAM-1-targeted nanoparticle accumulation in atherosclerotic ApoE$^{-/-}$ (top) and wild-type control (bottom) kidneys, imaged at 11.7T. Voxels with a signal intensity greater than twice the standard deviation were defined as positive for ^{19}F to produce a distribution map of ^{19}F throughout each kidney, which corresponds to nanoparticle binding via VCAM targeting.

VCAM-1 labelling was more sparse, limited to parietal epithelial cells of the Bowman's capsule and low level expression in the endothelium of larger capillaries, comparable to that previously observed in control kidney.[11] PECAM expression was also elevated in ApoE$^{-/-}$ kidney, but to a lesser extent than that observed for VCAM-1, indicative of a modest induction of angiogenesis in this model. Infiltration of macrophages into the capillaries of the Bowman's capsule was evident in ApoE$^{-/-}$ kidney, as delineated by Mac-2 staining, while very few macrophages were present in control kidneys (2.6 ± 2.0% vs 1.0 ± 0.2%, $P < .05$).

Nanobeacon biodistribution by fluorescence microscopy

Nanoparticle biodistribution within each kidney section was visualised using fluorescence microscopy to detect the nanoparticles' rhodamine content (Figure 5). The increased fluorescence we observed in the glomeruli and arterioles of the ApoE$^{-/-}$ kidney corresponded well to the regional staining for VCAM-1 we found in these kidneys (Figures 4 and 5 respectively), while very little such fluorescence was present in wild type control kidneys (Figure 5), reflecting the low levels of VCAM-1 expression we observed in healthy control tissue (Figure 4). These findings confirm the successful tracking and binding of our nanobeacons to the sites of increased VCAM-1 expression.

Quantitative analysis of VCAM-1 targeting by ^{19}F MR spectroscopy

Representative ^{19}F NMR spectra from kidneys are shown in Figure 1. The CE-cored nanoparticles gave rise to a single peak at -4 p.p.m., which did not overlap with the peaks corresponding to the PFOB spectrum, used as an internal standard for quantification purposes. Kidneys from ApoE$^{-/-}$ mice injected with VCAM-1-targeted nanoparticles were characterised by a strong peak at -4 p.p.m., corresponding to CE nanoparticles. This peak at -4 p.p.m. was present, but smaller in magnitude, in kidneys from ApoE$^{-/-}$ mice injected with non-targeted nanoparticles, and wild-type mice injected with VCAM-1-targeted nanoparticles. A standard calibration curve was generated from the relative peak areas of increasing concentrations of CE nanoparticles with a PFOB internal standard acquired using the same acquisition parameters, revealing an excellent linear correlation: $R^2 = 0.96$ (not shown). Based on this calibration reference, absolute nanoparticle numbers that had accumulated in each kidney were calculated and expressed per gram of kidney tissue, summarised in Figure 6. VCAM-1-targeted nanoparticles accumulated in ApoE$^{-/-}$ kidneys to a significantly greater (around four-fold) extent than did non-targeted nanoparticles (36.6 ± 8.8 vs. 9.3 ± 2.2 × 10^8/g wet weight, $P < .05$). ApoE$^{-/-}$ kidneys also manifested greater ^{19}F signal and accumulation of targeted nanoparticles than did non-ApoE$^{-/-}$ kidneys (36.6 ± 8.8 vs. 15.6 ± 2.3 vs. 15.4 ± 1.9 × 10^8/g wet weight, for ApoE$^{-/-}$ targeted vs. control targeted vs. control non-targeted, respectively, $P < .05$). No significant difference was observed between uptake of targeted versus non-targeted nanoparticles in kidneys from wild-type (control, non-ApoE$^{-/-}$) mice.

Nanoparticle biodistribution by magnetic resonance imaging

To provide examples of imaging readouts for *localized* detection of nanobeacon targeting, ^{1}H and ^{19}F images of

kidneys from ApoE$^{-/-}$ and C57/Bl6 mice injected with VCAM-1-targeted nanoparticles were acquired at 11.7T (Figure 7). The ^{19}F signal in ApoE$^{-/-}$ kidneys from mice injected with targeted nanoparticles was greater than that observed in kidneys from those injected with non-targeted nanoparticles, correlating well with the 4-fold increase in nanoparticle accumulation we calculated from our spectroscopy data, and provided a satisfactory signal-to-noise ratio of 3.0. The relative extent and distribution of the nanoparticles imaged by MRI was comparable to the distribution patterns of VCAM-1 obtained by immunohistochemistry, and agreed well with the nanoparticle distributions we observed using fluorescence microscopy.

Discussion

Several novel observations pertinent to clinical translation are reported in this work. First, we describe the *in vivo* use of a targetable nanobeacon displaying a unique MR signature which has great potential for the non-invasive diagnosis of pathophysiologically relevant biomarkers. Second, we demonstrate the capacity of this nanobeacon to enable quantification of the expression of VCAM-1, a critical mediator of inflammation particularly relevant to renal disease. Third, we illustrate a good correlation between the spectroscopic data we obtained with histological indices of renal inflammation that are normally only available clinically via biopsy. Fourth, we demonstrate our ability to visualise the biodistribution of VCAM-1 in intact kidneys by ^{19}F MR imaging.

The targeted MR nanobeacon we describe here is very versatile with respect to imaging and spectroscopy of ligand-targeted reporter agents. It is a lipid-encapsulated, liquid perfluorocarbon nanoparticle, with a nominal diameter range of 200-350 nm, which can be functionalised with many types of homing ligands in its outer phospholipid monolayer. This agent can provide multispectral MR contrast by incorporating either a large payload of paramagnetic Gd^{3+} nuclei (90,000+ per nanoparticle) on its surface,[12] or a 100M ^{19}F per nanoparticle payload in its core[13] (Figure 1, A). Traditional MR contrast agents (gadolinium- or iron oxide-based) operate by influencing water proton relaxivities to signal their presence, but such agents may be obscured by the background proton signals emanating from surrounding tissues, which makes delineation and quantification of their biodistribution difficult. This reporter agent, however, utilizes a ^{19}F signature, which manifests unique features for both imaging and spectroscopy[14]; its natural concentration in biological tissue is well below the sensitivity of MRS, meaning that any ^{19}F signal detected *in vivo* can only have originated from the nanoparticles that were exogenously introduced. This absence of background signal greatly facilitates image interpretation and absolute quantification by ^{19}F NMR spectroscopy, as we demonstrate. Furthermore, since a variety of perfluorocarbon core formulations can be distinguished by MR spectroscopy at clinically relevant field strengths (due to ^{19}F's large 300ppm chemical shift range), an array of nanobeacons containing distinct fluorine signatures (CE, PFOB, perfluorodecalin, etc.) can be formulated that might be individually labelled but simultaneously quantified to track several biological processes simultaneously.[15,16] In this application, we utilise nanoparticles filled with perfluoro-15-crown-5-ether, which contains 20 equivalent fluorine nuclei, giving rise to a single easily identifiable MR peak (Figure 1, B), for specific and sensitive quantification and visualisation of VCAM-1 epitopes.

VCAM-1 is primarily responsible for the tethering of leukocytes to the vascular lumen during the inflammatory response (for review see Postigo *et al*[17]). In the kidney, VCAM-1 has been implicated in the pathogenesis of numerous disease processes,[18] including allograft rejection,[19] diabetic nephropathy,[20] lupus[21] and chronic renal failure.[22] Increased VCAM-1 expression precedes macrophage infiltration and foam cell formation, indicating that VCAM-1 up-regulation is a very early step in the onset of atherosclerotic lesion formation.[23] VCAM-1 blockade has been shown to significantly reduce atherosclerotic lesion development, and prolong renal and cardiac allograft tolerance,[24,25] confirming VCAM-1′s pivotal role in these processes, and further demonstrating its potential as an important molecular imaging biomarker for renal pathology.

The VCAM-1 targeting peptide $VINP_{28}$, first reported by Kelly *et al*,[7] shows sequence homology to very late antigen 4 (VLA-4). $VINP_{28}$ has been previously shown to specifically bind to VCAM-1 and block leukocyte-endothelial interaction,[7] and has recently been used to target iron oxide nanoparticles to macrophages in atherosclerotic lesions in mouse aorta,[26] We demonstrate that the accumulation of our $VINP_{28}$-targeted lipid-perfluorocarbon nanoparticles on endothelium was 4-fold greater in ApoE$^{-/-}$ kidneys than in wild-type kidneys, which mirrors the relative ratios we, and others,[3] observe between ApoE$^{-/-}$ and wild-type kidneys for the expression of VCAM-1 itself.

The prodigious capacity of macrophages for phagocytosis and receptor-mediated endocytosis has made them prime targets for MRI-based approaches for the visualisation of inflammation. While this capacity may be advantageous for imaging inflammation in general, it can be an obstacle to the *specific* imaging of other intravascular targets, particularly in disease states associated with large numbers of macrophages. While macrophage infiltration represents a useful imaging biomarker, it is not as specific, or as early, or as temporally distinct, as endothelial VCAM-1 expression.[27] We show that 2 hours post-injection, there is no difference between the non-targeted nanoparticle retention in the ApoE$^{-/-}$ kidney and the normal kidney, despite the markedly greater macrophage population in the ApoE-null kidney, as quantified by Mac-2 expression

(Figure 4). At this time-point therefore, the signal we observe is specific to VCAM-1, and unaffected by macrophage activity.

While the data we present here demonstrate our capacity for *in vivo* nanoparticle targeting to VCAM-1, this study does not extend directly to the visualisation of these nanoparticles *in vivo*. Additional work on coil design and sequence optimization is underway to perform these measurements *in vivo* at 3T. We have previously demonstrated successful *in vitro* and *in vivo* imaging and spectroscopy of ^{19}F nanobeacons on clinical 1.5T and 3T systems for various purposes such as angiography, stem cell imaging, and thrombus detection,[15,16,28] and anticipate that the use of targeted ^{19}F nanobeacons for quantifying inflammation in situations such as the metabolic syndrome would represent promising clinical subjects of future investigation. The correlation between our "non-invasive" spectroscopy and imaging data and our "invasive" histologic data demonstrates its promise as a surrogate for kidney biopsy, with the additional benefit of allowing non-invasive longitudinal monitoring of renal inflammation and transplantation rejection management. Finally, the potential to use these nanoparticle carriers as site-targeted drug delivery vehicles and diagnostic devices simultaneously, as we have previously demonstrated,[29] offers considerable promise for rational drug dosing and follow-up of therapeutic strategies to prevent or cure kidney disease.

References

1. Peppa M, Uribarri J, Cai W, Lu M, Vlassara H. Glycoxidation and inflammation in renal failure patients. Am J Kid Dis 2004;43(4):690-5.
2. Longenecker JC, Klag MJ, Marcovina SM, Powe NR, Fink NE, Giaculli F, et al. Choices for Healthy Outcomes in Caring for ESRD. Small apolipoprotein(a) size predicts mortality in end-stage renal disease. Circulation 2002;106(22):2812-8.
3. Bruneval P, Bariety J, Belair MF, Mandet C, Heudes D, Nicoletti A. Mesangial expansion associated with glomerular endothelial cell activation and macrophage recruitment is developing in hyperlipidaemic apoE null mice. NephrolDialTrans 2002;17(12):2099-107.
4. Lin J, Hu FB, Rimm EB, Rifai N, Curhan GC. The association of serum lipids and inflammatory biomarkers with renal function in men with type II diabetes mellitus. Kidney Intl 2006;69(2):336-42.
5. Bolton CH, Downs LG, Victory JG, Dwight JF, Tomson CR, Mackness MI, et al. Endothelial dysfunction in chronic renal failure: roles of lipoprotein oxidation and pro-inflammatory cytokines. NephrolDialTrans 2001;16(6):1189-97.
6. Winter PM, Caruthers SD, Kassner A, Harris TD, Chinen LK, Allen JS, et al. Molecular imaging of angiogenesis in nascent Vx-2 rabbit tumors using a novel alpha(nu)beta3-targeted nanoparticle and 1.5 tesla magnetic resonance imaging. Cancer Res 2003;63(18):5838-43.
7. Kelly KA, Allport JR, Tsourkas A, Shinde-Patil VR, Josephson L, Weissleder R. Detection of vascular adhesion molecule-1 expression using a novel multimodal nanoparticle. Circ Res 2005;96(3):327-36.
8. Walter-Yohrling J, Morgenbesser S, Rouleau C, Bagley R, Callahan M, Weber W, et al. Murine endothelial cell lines as models of tumor endothelial cells. Clin Canc Res 2004;10(6):2179-89.
9. Morawski AM, Winter PM, Yu X, Fuhrhop RW, Scott MJ, Hockett F, et al. Quantitative "magnetic resonance immunohistochemistry" with ligand-targeted (19)F nanoparticles. Magn Res Med 2004;52(6):1255-62.
10. Clark Jr LC, Ackerman JL, Thomas SR, Millard RW, Hoffman RE, Pratt RG, et al. Perfluorinated organic liquids and emulsions as biocompatible NMR imaging agents for ^{19}F and dissolved oxygen. Adv Exp Med Biol 1984;180:835-45.
11. Allen AR, McHale J, Smith J, Cook HT, Karkar A, Haskard DO, et al. Endothelial expression of VCAM-1 in experimental crescentic nephritis and effect of antibodies to very late antigen-4 or VCAM-1 on glomerular injury. J Immunol 1999;162(9):5519-27.
12. Winter PM, Morawski AM, Caruthers SD, Fuhrhop RW, Zhang H, Williams TA, et al. Molecular imaging of angiogenesis in early-stage atherosclerosis with alpha(v)beta3-integrin-targeted nanoparticles. Circulation 2003;108(18):2270-4.
13. Morawski AM, Winter PM, Crowder KC, Caruthers SD, Fuhrhop RW, Scott MJ, et al. Targeted nanoparticles for quantitative imaging of sparse molecular epitopes with MRI. Magn Res Med 2004;51(3):480-6.
14. Yu JX, Kodibagkar VD, Cui W, Mason RP. ^{19}F: a versatile reporter for non-invasive physiology and pharmacology using magnetic resonance. Curr Med Chem 2005;12(7):819-48.
15. Caruthers SD, Neubauer AM, Hockett FD, Lamerichs R, Winter PM, Scott MJ, et al. In vitro demonstration using ^{19}F magnetic resonance to augment molecular imaging with paramagnetic perfluorocarbon nanoparticles at 1.5 Tesla. Invest Radiol 2006;41(3):305-12.
16. Partlow KC, Chen J, Brant JA, Neubauer AM, Meyerrose TE, Creer MH, et al. ^{19}F magnetic resonance imaging for stem/progenitor cell tracking with multiple unique perfluorocarbon nanobeacons. FASEB J 2007;21(8):1647-54.
17. Postigo AA, Teixido J, Sanchez-Madrid F. The alpha 4 beta 1/VCAM-1 adhesion pathway in physiology and disease. Res Immunol 1993;144(9):723-35.
18. Rabb H, Rosen R, Ramirez G. VLA-4 and its ligands: relevance to kidney diseases. Springer Seminars in Immunopathology 1995;16(4):417-25.
19. Kauppinen H, Soots A, Krogerus L, Loginov R, Holma K, Ahonen J, et al. Sequential analysis of adhesion molecules and their ligands in rat renal allografts during the development of chronic rejection. Transpl Internat 2000;13(4):247-54.
20. Chang CJ, Ko YS, Ko PJ, Hsu LA, Chen CF, Yang CW, et al. Thrombosed arteriovenous fistula for hemodialysis access is characterized by a marked inflammatory activity. Kidney Internat 2005;68(3):1312-9.
21. Nakatani K, Fujii H, Hasegawa H, Terada M, Arita N, Ito MR, et al. Endothelial adhesion molecules in glomerular lesions: association with their severity and diversity in lupus models. Kidney Internat 2004;65(4):1290-300.
22. Malyszko J, Malyszko JS, Myliwiec M. Endothelial cell injury markers in chronic renal failure on conservative treatment and continuous ambulatory peritoneal dialysis. Kidn & Blood Press Res 2004;27(2):71-7.
23. Dansky HM, Barlow CB, Lominska C, Sikes JL, Kao C, Weinsaft J, et al. Adhesion of monocytes to arterial endothelium and initiation of atherosclerosis are critically dependent on vascular cell adhesion molecule-1 gene dosage. Arterio Thromb Vasc Biol 2001;21(10):1662-7.
24. Orosz CG, Bergese SD, Huang EH, Vanbuskirk AM. Immunologic characterization of murine cardiac allograft recipients with long-term graft survival due to anti-VCAM-1 or anti-CD4 monoclonal antibody therapy. Transpl Proc 1995;27(1):387-8.
25. Isobe M, Suzuki J, Yagita H, Okumura K, Yamazaki S, Nagai R, et al. Immunosuppression to cardiac allografts and soluble antigens by anti-vascular cellular adhesion molecule-1 and anti-very late antigen-4 monoclonal antibodies. J Immunol 1994;153(12):5810-8.
26. Kelly KA, Nahrendorf M, Yu AM, Reynolds F, Weissleder R. In vivo phage display selection yields atherosclerotic plaque targeted peptides for imaging. Molec Im Biol 2006;8(4):201-7.
27. Sakai A, Kume N, Nishi E, Tanoue K, Miyasaka M, Kita T. P-selectin and vascular cell adhesion molecule-1 are focally expressed in aortas of

hypercholesterolemic rabbits before intimal accumulation of macrophages and T lymphocytes. Arterio Thromb Vasc Biol 1997;17(2): 310-6.

28. Neubauer AM, Caruthers S, Hockett FD, Cyrus T, Robertson JD, Allen JS, et al. Fluorine MR angiography in vivo at 1.5 T with perfluorocarbon nanoparticle contrast agents. J Cardiovasc Mag Res 2007;9(3):565-73.
29. Wickline SA, Neubauer AM, Winter PM, Caruthers SD, Lanza GM. Molecular imaging and therapy of vascular targets with targeted nanoparticles. J Mag Res Imag 2007;25:667-80.